Available online at www.sciencedirect.com
ScienceDirect
Polymer 48 (2007) 4520–4528
polymer
www.elsevier.com/locate/polymer

The dynamics of montmorillonite clay dispersion and morphology development in immiscible ethylene–propylene rubber/polypropylene blends

Marianna Kontopoulou*, Yiqun Liu, Jeremy R. Austin, J. Scott Parent

Department of Chemical Engineering, Queen's University, Kingston, ON K7L 3N6, Canada

Received 5 February 2007; received in revised form 16 May 2007; accepted 20 May 2007
Available online 2 June 2007

Abstract

The evolution of morphology during the melt compounding of polypropylene (PP), maleated ethylene–propylene rubber (EPR-*g*-MAn) and onium-ion exchanged montmorillonite clay (NR_4^+-MM) is described. Irrespective of the ratio of components, clay partitions into the EPR-*g*-MAn phase exclusively, with significant amounts of mineral exfoliation occurring in the very early stages of compounding. These changes in filler distribution and dispersion are accompanied by reductions in the size of the dispersed PP phase, as the rate of droplet coalescence falls in response to an elevated EPR-*g*-MAn matrix viscosity. However, when NR_4^+-MM is localized in a dispersed EPR-*g*-MAn phase, coalescence increases as a result of hindered particle break-up.

Keywords: Blends; Nanocomposites; Morphology

1. Introduction

The effect of nanofillers on the structure and properties of immiscible and partially miscible polymer blends has been the topic of intense recent investigation [1–19]. Exfoliated clay platelets and nanoscale silica particles have dimensions comparable to, or smaller than, the domain sizes of many multiphase blends. As a result, they can influence the structural development of blends during melt processing and cause substantial reductions in the size of dispersed domains [1–13,19].

Theories that describe these effects vary, depending on whether the filler is located in the continuous phase, in the dispersed phase, or at the interphase between the two blend components. Filler-induced changes in the interfacial tension between polymer components [4] have been suggested in the context of an emulsifying/compatibilizing effect [4,12]. The possibility that exfoliated clay platelets may hinder particle coalescence by acting as physical barriers has also been proposed [2,5,8]. Others have noted that the high viscosity of clay-containing matrices may improve stress transfer to the dispersed phase and/or retard droplet coalescence during compounding [6,8,9]. The resulting changes in the viscosity ratio are expected to affect the balance between droplet break-up and coalescence [13]. The potential for rigid clay particles to reinforce the interface has also been presented as a contributing factor for reductions in the rate of particle break-up [9,11].

The development of blend morphology in a nanocomposite system is affected by continuous changes in filler distribution and dispersion. We have reported that onium-ion exchanged montmorillonite clay (NR_4^+-MM) partitions exclusively into an EPR-*g*-MAn matrix when these two materials are compounded simultaneously with PP for several minutes [19]. Furthermore, the clay exists primarily as exfoliated platelets in these fully developed nanocomposite blends. Although the

* Corresponding author. Tel.: +1 613 533 3079; fax: +1 613 533 6637.
E-mail address: marianna.kontopoulou@chee.queensu.ca (M. Kontopoulou).

0032-3861/$ - see front matter © 2007 Elsevier Ltd. All rights reserved.
doi:10.1016/j.polymer.2007.05.068

location and state of a nanofiller are generally believed to affect the dynamics of droplet break-up and coalescence, detailed accounts of this process are lacking. This report describes experimental studies of the evolution of dispersed phase size, filler partitioning, and clay aggregate dispersion during melt compounding of PP/EPR-*g*-MAn/NR_4^+-MM composites. These data are, in turn, discussed in the context of proposed theories of morphology development.

2. Experimental

2.1. Materials

A montmorillonite clay, NR_4^+-MM (Nanomer® I.44PA), ion-exchanged with dimethyl dialkylammonium halide (70% C_{18}, 26% C_{16}, and 4% C_{14}) was supplied by Nanocor Inc., located in Arlington Heights, Illinois, and was used as received. Polypropylene (PP, Escorene PP1042, MFR 1.9 g/10 min at 230 °C) was supplied by ExxonMobil Chemical. A maleated ethylene-*co*-propylene copolymer (EPR-*g*-MAn, Fusabond® MF-416D, MFI 23 g/10 min at 280 °C, density 870 kg/m^3) containing 0.5–1.0 wt% maleic anhydride was obtained from E.I. DuPont Canada. Irganox B225 antioxidant was obtained from Ciba–Geigy.

2.2. Composite preparation

Blends containing EPR-*g*-MAn and PP at ratios of 70/30 and 30/70 by weight were prepared in a Haake PolyLab torque rheometer, which was connected to a Rheomix 610p mixing chamber equipped with roller rotors. The instrument was operated at 60 rpm at a fill factor of 70% and a compounding temperature of 200 °C. Preliminary experiments revealed that the morphology of the blends did not change significantly after 4 min of compounding. Therefore the polymers were compounded for 4 min prior to the addition of the filler, until steady-state torque was achieved and for an additional 4 min once the filler was added.

2.3. Wide-angle X-ray scattering

The basal spacing of the clays in the composites was evaluated by wide-angle X-ray scattering (WAXS) using a Scintag Model X1 powder X-ray diffractometer (Cu Kα radiation, $\lambda = 1.5406$ Å, generator voltage = 45 kV, current = 40 mA). Films of approximately 400 nm thick were prepared using a hot press and scanned in a 2θ range from 1° to 50° at a rate of 1°/min. Measurements were recorded at every 0.03° interval.

2.4. Transmission electron microscopy (TEM)

A FEI Tecnai 20 TEM (200 kV) transmission electron microscope was used to characterize the structure of all the composites. The samples were sectioned with a diamond knife on a Leica ultracut cryo-ultramicrotome at −100 °C to yield specimens of approximately 70 nm in thickness that were then placed on formvar coated copper grids. Microtomed sections from the nanocomposite blends were collected on carbon-coated copper grids and held in the vapour of 0.5% RuO_4 for 1 h to enhance the compositional contrast between the phases. Photographs of the samples were obtained using a Gatan Dualview digital camera.

2.5. Scanning electron microscopy (SEM)

Surfaces for SEM were prepared by fracturing the samples under liquid nitrogen. The specimens were sputtered with gold and observed using a JEOL 840 scanning electron microscope. Elemental analysis was performed using Electron Diffraction Spectrometry (EDS) to confirm the presence of clay aggregates in the composites. The number and volume average sizes of the particles of the dispersed phase were determined by performing image analysis on the SEM images with Sigma-Scan Pro image analysis software.

2.6. Rheological characterization

Compression-molded disks were used for rheological characterization. The elastic modulus (G'), loss modulus (G''), and complex viscosity (η^*) were measured as a function of angular frequency (ω) using a Reologica ViscoTech oscillatory rheometer. The rheometer was operated in the dynamic oscillatory mode with parallel plate fixtures of 20 mm in diameter and at a gap of 1.5 mm. All the tests were carried out under a nitrogen blanket to limit the degree of polymer degradation and moisture absorption. Strain sweeps were performed to verify that the measurements were within the linear viscoelastic region. Steady-shear viscosity measurements were done using a Rosand RH2000 Dual Bore Capillary rheometer at a temperature of 200 °C. The Rabinowitch and Bagley corrections were employed to calculate the corrected shear stress and shear rate data. For all rheological characterization the average of three independent measurements is reported.

2.7. Evaluation of bound polymer content

Chopped EPR-*g*-MAn/clay composite (1 g) was dissolved in toluene (40 ml) at 80 °C. After cooling, the solution was subjected to centrifugal separation at 4000 rpm for 1 h. The supernatant was decanted, and the solids were shaken with 30 ml of fresh toluene before being left to stand for 2 h. Centrifugal separation was repeated and the remaining solids (containing NR_4^+-MM and bound polymer) were dried under vacuum at 60 °C.

Bound polymer determinations were made using a TA Instruments Q500 Series thermogravimetric analysis instrument to heat the samples from 25 °C to 650 °C under a nitrogen atmosphere at a rate of 10 °C/min. Percent weight losses were recorded for NR_4^+-MM, an unextracted sample of EPR-*g*-MAn nanocomposite containing 5 wt% NR_4^+-MM, and the solids were extracted from this material.

3. Results and discussion

3.1. EPR-g-MAn rich blends

We begin with an examination of blends that are rich in EPR-*g*-MAn. This series of experiments involved compounding a 70/30 EPR-*g*-MAn/PP blend for 4 min, to ensure that the components were fully molten and a stable morphology had been reached prior to adding 5 wt% of NR_4^+-MM. Fig. 1 illustrates the morphology of the initially unfilled blend, as well as the morphology of the filled system after 1 min, 2 min, and 4 min of compounding with clay.

The SEM image illustrated in Fig. 1a reveals the droplet-matrix morphology of the unfilled blend, whose steady-state, number average particle diameter was $d_n = 2.33 \pm 0.83$ μm. We note that this diameter is significantly larger than that observed for a 90/10 blend of these materials (not shown), which arrives at an average diameter of $d_n = 0.85 \pm 0.17$ μm. This suggests that the unfilled EPR-*g*-MAn/PP blends are prone to dispersed phase coalescence at the relatively high PP contents used here. More importantly, the addition of 5 wt% of NR_4^+-MM resulted in a rapid reduction in the size of PP domains. Substantial differences were observed after just 1 min of compounding with clay (Fig. 1b), while after 3 min of mixing, the PP droplets reduced to a mean diameter of 0.5 ± 0.17 μm (Fig. 1d).

SEM analysis of these materials at lower magnification provided information regarding the state of clay aggregates during compounding (Fig. 2). After 1 min of mixing NR_4^+-MM into the blend, clay particles with dimensions in the order of 20 μm were observed. However, their number decreased with continued processing to the point where aggregates were relatively scarce at the 4 min mark. In fact, wide-angle X-ray scattering (WAXS) profiles of this material showed no evidence of the characteristic diffraction peak derived from native NR_4^+-MM (Fig. 3).

Further insight into the state of the distribution and dispersion of the clay filler was gained through TEM imaging. Fig. 4 shows the evolution of the blend toward a final state where NR_4^+-MM is localized within the EPR matrix and PP exists as an unfilled dispersed phase.

This result is similar to that obtained previously [19] where all components were compounded simultaneously. Furthermore, we observed migration of NR_4^+-MM to the functionalized phase when EPR-*g*-MAn was added to a molten PP/NR_4^+-MM masterbatch. Therefore the preferential partition of NR_4^+-MM into the EPR-*g*-MAn is not due to the big difference in the melting points of the two components and the process is not kinetically controlled, since the processing method does not affect the distribution of the filler.

Previous research on carbon black fillers has shown that the filler distribution in a binary blend is controlled by the balance

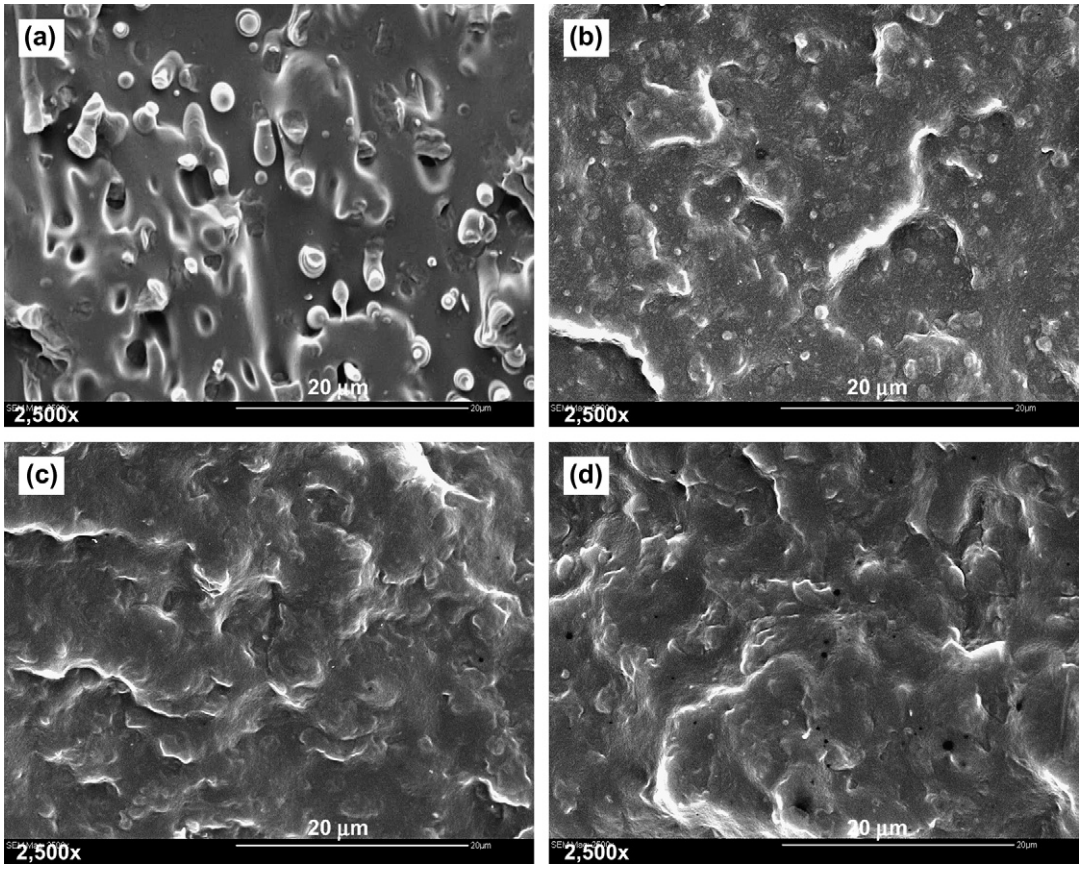

Fig. 1. SEM images showing the evolution of morphology at various compounding times, upon addition of 5 wt% NR_4^+-MM in a pre-compounded 70/30 EPR-*g*-MAn/PP blend (a) unfilled blend; filled blend after (b) 1 min; (c) 2 min; (d) 4 min. Scale bars correspond to 20 μm.

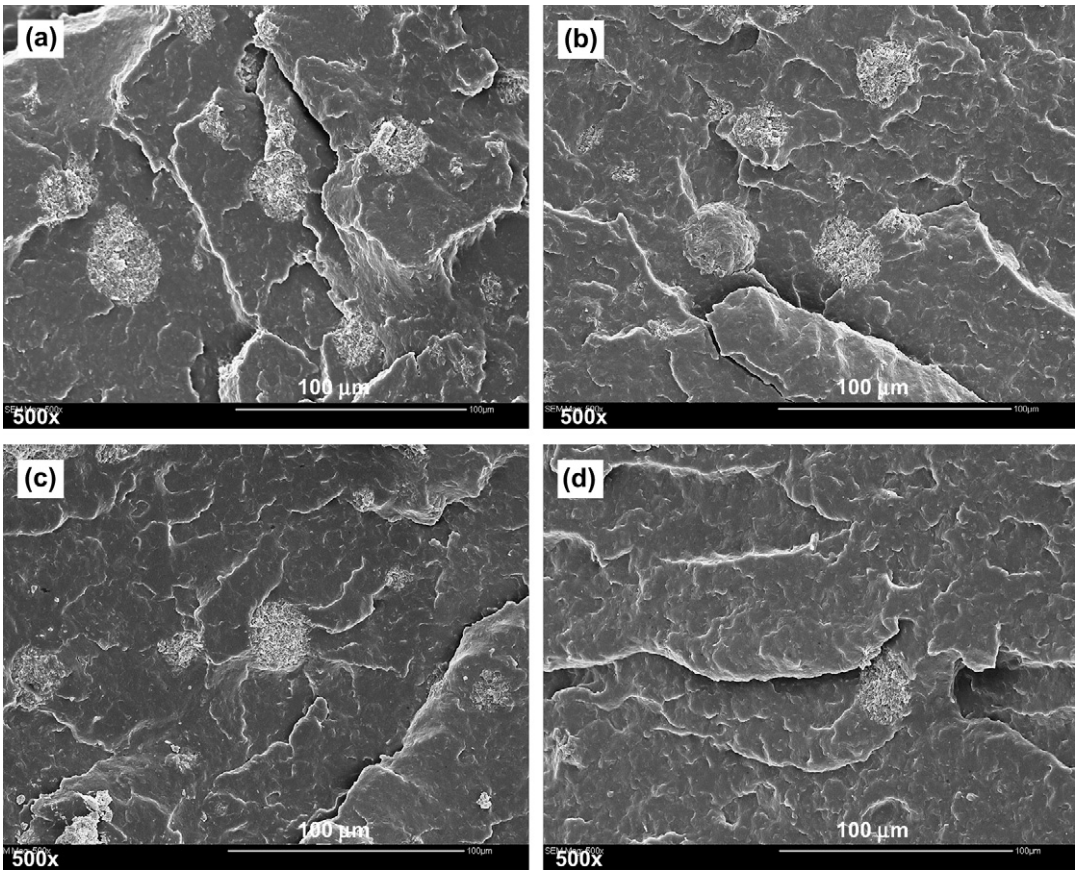

Fig. 2. SEM images of PP/EPR-*g*-MAn/clay composites depicting clay aggregate break-up at various compounding times, upon addition of 5 wt% NR_4^+-MM in a pre-compounded 70/30 EPR-*g*-MAn/PP blend (a) 1 min; (b) 2 min; (c) 3 min; (d) 4 min. Scale bars correspond to 100 µm.

of the interactions of the filler with each constitutive polymeric component and is dictated by the state of the minimum interfacial energy, when all other parameters, such as viscosity of the blend components, are comparable [20,21].

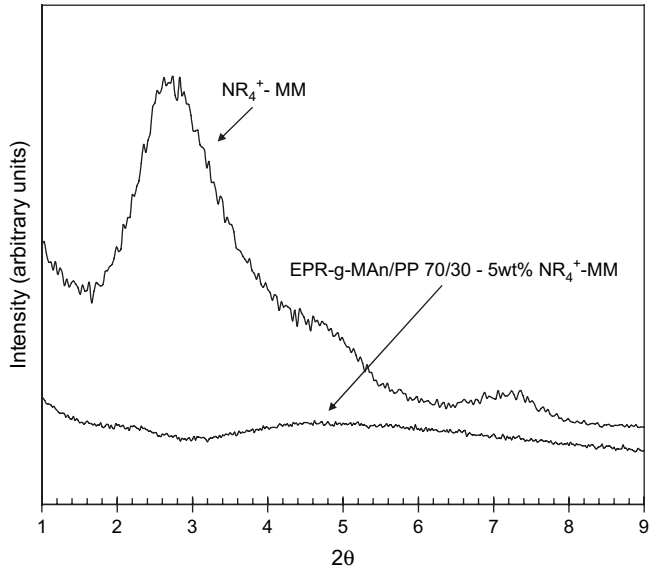

Fig. 3. WAXS diffraction patterns of organoclay and EPR-*g*-MAn/PP 70/30 blend containing 5 wt% NR_4^+-MM.

Apparently in polyolefin blends such as the ones under consideration in this work, this thermodynamic condition is met when the filler is localized exclusively within the functionalized phase.

The TEM images shown in Fig. 4 demonstrate that the clay lost from large aggregates exists in the form of exfoliated platelets, as well as small intercalated tactoids. This suggests that upon loading the clay into an already compounded PP/EPR-*g*-MAn blend, the aggregates start to split as they are subjected to shearing and clay platelets become separated upon coming into contact with the functionalized component. This gives rise to a significant amount of exfoliated clay platelets at the very early stages of compounding (Fig. 4b). Presence of exfoliated clay platelets in the EPR-*g*-MAn matrix in the early stages of mixing can contribute to matrix properties and, by extension, to blend morphology development.

The rheological data presented in Fig. 5 reveal the remarkable effect of a small dispersed clay population on the melt flow properties of the blend. Significant increases in complex viscosity and elastic modulus were realized within 1 min of compounding, with only marginal gains observed at longer compounding times.

A comparison of SEM, TEM and rheological data reveals a coincidence of clay platelet dispersion, PP droplet size reduction, and melt-state properties. Although NR_4^+-MM dispersion was not complete within 1 min of processing, the presence of

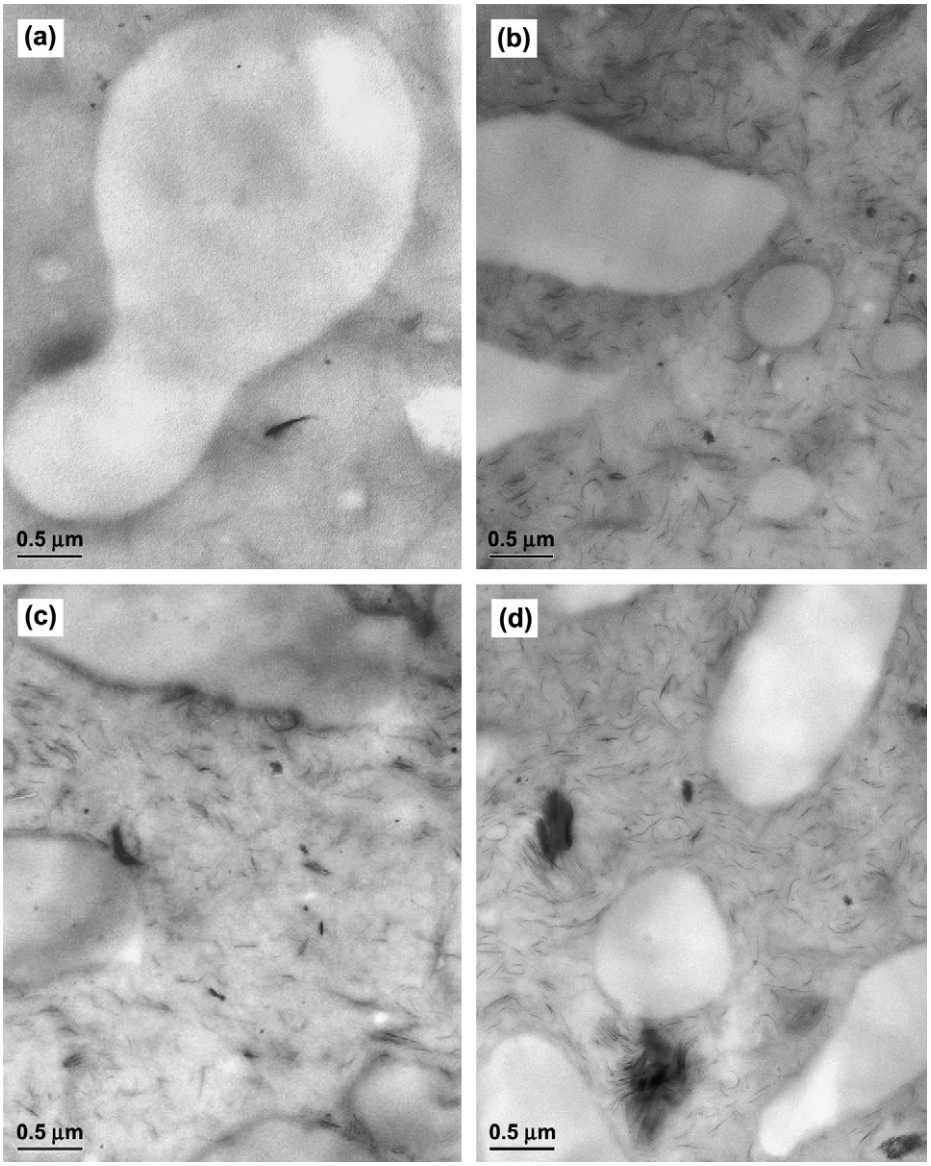

Fig. 4. TEM images depicting the state of the clay dispersion at various compounding times, upon addition of 5 wt% NR_4^+-MM in a pre-compounded 70/30 EPR-*g*-MAn/PP blend (a) unfilled blend; filled blend after (b) 1 min; (c) 2 min; (d) 4 min. The elastomer phase is stained and appears darker.

exfoliated clay had a direct and significant effect on the evolution of blend characteristics. After 4 min of mixing, extensive NR_4^+-MM delamination and dispersion was achieved, and the blend achieved a stable morphology and an unvarying viscosity.

Knowledge of the state of filler partitioning allows us to estimate the rheological properties of the individual components of the composite blends, as well as their interfacial tensions and compare them with respective properties of the components of an unfilled blend. Specifically, based on our findings, an EPR-*g*-MAn/PP 70/30 blend containing 5 wt% NR_4^+-MM consisted of an EPR-*g*-MAn matrix containing 7 wt% NR_4^+-MM and an unfilled dispersed phase. Based on this a series of complimentary experiments were completed to provide further insight into the development of nanocomposite blend structure, the results of which are detailed below.

3.1.1. Rheological effects on droplet break-up and coalescence

Recognizing that the balance between droplet break-up and coalescence dictates blend morphology, the potential influence of component rheology was examined. It is well known that droplet break-up is dependent on the viscosity ratio, the matrix viscosity, and the shear rate experienced during compounding.

The combined oscillatory and steady-shear viscosity data presented in Fig. 6a reveal the extent that exfoliated clay increases the viscosity of EPR-*g*-MAn. It should be noted that although the unfilled components follow the Cox–Merz rule, the same does not hold true for the filled EPR-*g*-MAn. The increase in the viscosity of the EPR-*g*-MAn matrix alters slightly the viscosity ratio at the entire shear rate range produced by a batch mixing device. For example, at a shear rate of 50 s^{-1}, the viscosity of PP relative to NR_4^+-MM reinforced

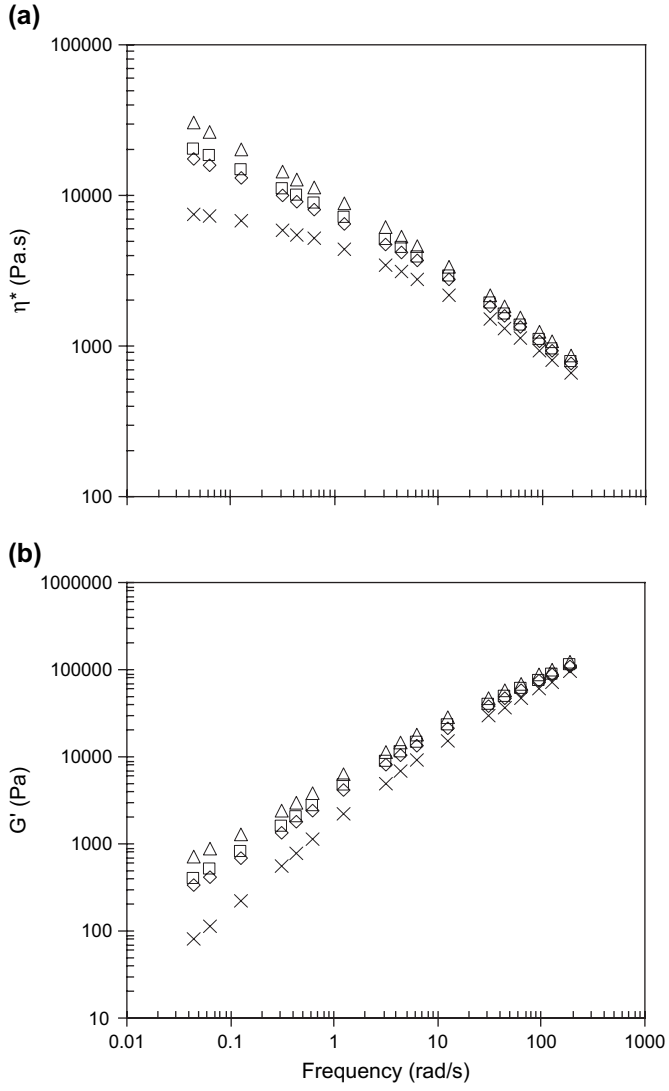

Fig. 5. (a) Complex viscosity (η^*) and (b) elastic modulus (G') as a function of frequency at 200 °C for unfilled 70/30 PP/EPR-*g*-MAn blend and NR_4^+-MM filled blends at different compounding times; × unfilled blend; ◇ 1 min; □ 2 min; △ 4 min.

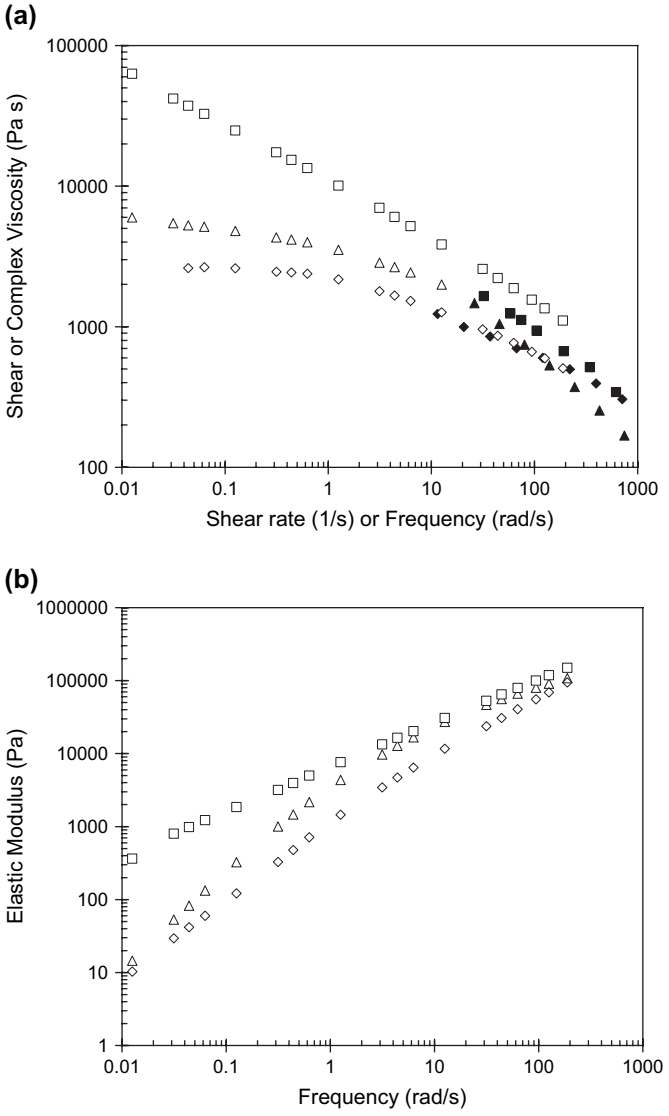

Fig. 6. Steady-shear and oscillatory data measured at 200 °C (a) combined shear viscosity and complex viscosity as a function of shear rate or frequency, respectively; (b) elastic modulus as a function of frequency for △ PP; ◇ EPR-*g*-MAn; □ EPR-*g*-MAn containing 7 wt% NR_4^+-MM. Open symbols denote oscillatory data and closed symbols represent data obtained using the capillary rheometer.

EPR-*g*-MAn was $\eta_{dispersed}/\eta_{matrix} = 0.9$, compared to a value of 1.2 for the unfilled system, which does not constitute a significant difference given the experimental error associated with these types of measurements. Additionally the matrix viscosity increased by 34%, which represents a much more significant change. Based on the model of droplet break-up proposed by Everaert et al. [22], these changes are expected to produce a 30% reduction of the dispersed particle size in blends where coalescence effects are negligible. By contrast our experimental evidence suggests a 78% reduction in particle size. This may be due to changes in the coalescence rate, attributed to the altered rheological properties of the matrix in the presence of exfoliated clay platelets.

In our system, in addition to the increase in matrix viscosity at high shear rates documented in Fig. 6a, we have observed dramatic increases in the low frequency complex viscosities and elastic moduli for NR_4^+-MM reinforced EPR-*g*-MAn (Fig. 6a and b). The significant increase in complex viscosity and melt elasticity in the presence of clay is well documented in the literature and has been frequently attributed to the formation of a network consisting of exfoliated clay platelets [27,28]. Polymer–filler interactions, resulting from the presence of polymer bound to the filler can also affect viscoelastic properties substantially [29]. We have examined the adsorption capacity of NR_4^+-MM platelets for EPR-*g*-MAn by extracting a 5 wt% NR_4^+-MM nanocomposite with hot toluene. Fig. 7 shows the weight losses recorded by TGA for NR_4^+-MM, an EPR-*g*-MAn nanocomposite containing 5 wt% NR_4^+-MM, and the solids extracted from it. Based on this data, a bound polymer content of 1.2 g of EPR-*g*-MAn per 1.0 g of NR_4^+-MM was recorded. The presence of bound polymer is consistent with the pronounced increase in the low shear

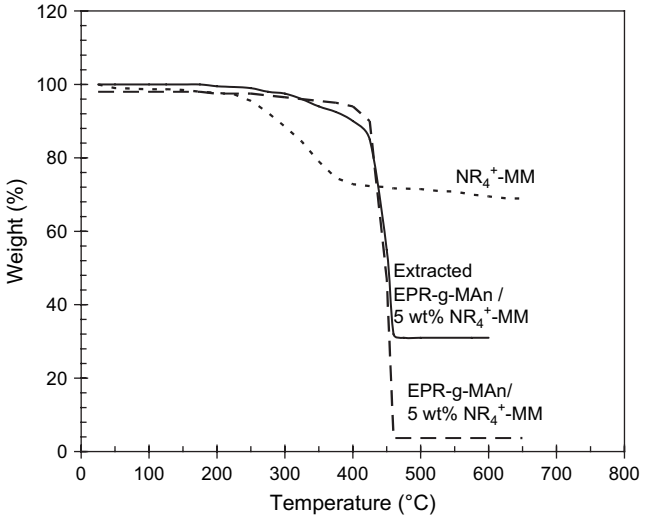

Fig. 7. TGA traces for NR_4^+-MM, an EPR-*g*-MAn nanocomposite containing 5 wt% NR_4^+-MM, and the solids extracted from the EPR-*g*-MAn/5 wt% NR_4^+-MM composite.

viscosity and elasticity data, and the deviations from terminal flow behaviour seen in Fig. 6 [29].

The existence of an immobilized layer, consisting of clay platelets and bound polymer, around the droplets of the dispersed phase may impose a physical barrier to droplet coalescence [2,5,8]. Furthermore, the reduced mobility of the confined polymer chains that are bound to the filler likely causes a decrease in the drainage rate of the thin film separating two droplets [23–26].

3.1.2. Interfacial tension effects

We have further considered the possibility that organoclay lowers the interfacial tension [4], thus creating a compatibilization effect similar to that of block copolymers [9,11]. However, contrary to previous reports where the clay migrates to the blend interface [4], in the system of present interest, the exfoliated filler resides in the bulk of the matrix phase, therefore it is not expected to affect interfacial properties. To further corroborate this hypothesis, we estimated the interfacial tensions of the unfilled and filled blends, using the Palierne emulsion model [30,31], shown in Eq. (1) for the simplified case, where the polydispersity, d_v/d_n, of the dispersed droplets is less than 2 [31].

$$G^*(\omega) = G_m^*(\omega)\frac{1+3\phi H^*(\omega)}{1-2\phi H^*(\omega)} \tag{1}$$

$$H^*(\omega) = \frac{8\left(\frac{\sigma}{d_v}\right)\left[2G_m^*(\omega)+5G_d^*(\omega)\right]+\left[G_d^*(\omega)-G_m^*(\omega)\right]\left[16G_m^*(\omega)+19G_d^*(\omega)\right]}{80\left(\frac{\sigma}{d_v}\right)\left[G_m^*(\omega)+G_d^*(\omega)\right]+\left[2G_d^*(\omega)+3G_m^*(\omega)\right]\left[16G_m^*(\omega)+19G_d^*(\omega)\right]} \tag{2}$$

where $G_m^*(\omega)$ is the complex modulus for matrix and $G_d^*(\omega)$ is the complex modulus for the dispersed phase (droplet), respectively, σ is the interfacial tension, ϕ is the volume fraction of dispersed phase and d_v is the volume average diameter of the droplets.

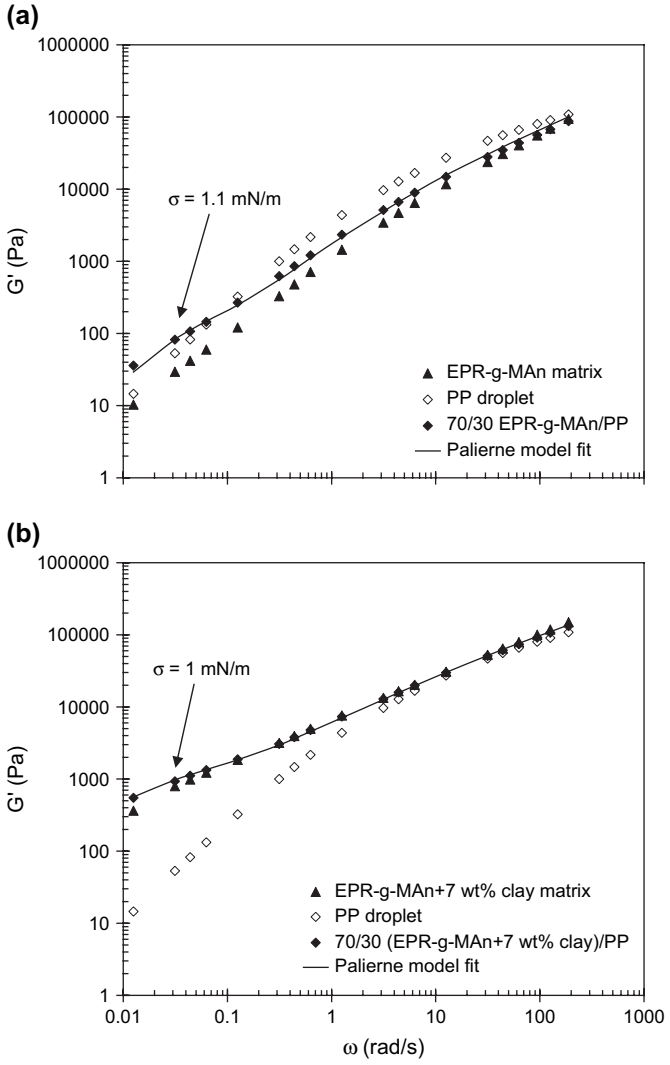

Fig. 8. (a) Palierne model fit for EPR-*g*-MAn/PP 70/30 blend; (b) Palierne model fit for model blend, which comprises an EPR-*g*-MAn matrix containing 7 wt% NR_4^+-MM and PP dispersed phase at a ratio of 70/30.

The model was first fit to the elastic modulus versus frequency profile of an unfilled 70/30 EPR-*g*-MAn/PP blend that had reached a stable morphology, starting from the known rheological properties of the base EPR-*g*-MAn and PP polymers and using a volume average diameter $d_v = 2.8$ μm (corresponding to a number average $d_n = 2.2$ μm, with $d_v/d_n = 1.27$). This produced a fitted value for the interfacial tension, $\sigma = 1.1$ mN/m (Fig. 8a). Since the exfoliated filler resides exclusively in the EPR-*g*-MAn matrix, we also formulated a model blend by preparing a composite of EPR-*g*-MAn with 7 wt% NR_4^+-MM, and compounding this material with PP in a ratio of (EPR-*g*-MAn + NR_4^+-MM)/PP 70/30 until a stable morphology had been achieved. The

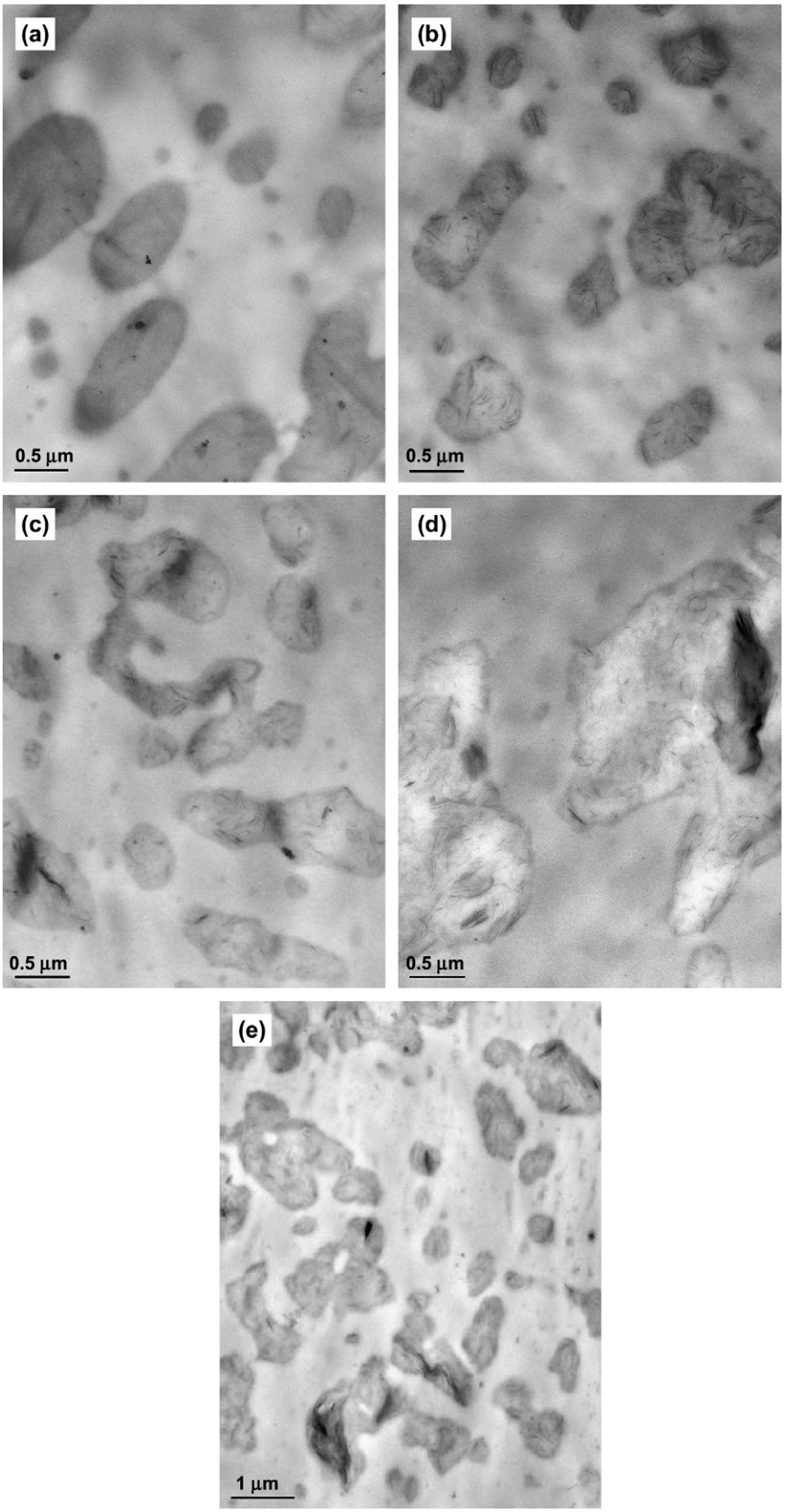

Fig. 9. Evolution of morphology at various compounding times, upon addition of 5 wt% NR_4^+-MM in a pre-compounded 30/70 EPR-*g*-MAn/PP blend; (a) unfilled blend; filled blend after (b) 1 min; (c) 2 min; (d and e) 4 min.

number and volume average diameters determined by SEM were $d_n = 0.6$ μm and $d_v = 1$ μm, respectively ($d_v/d_n = 1.67$). Application of the Palierne model, using the filled EPR-*g*-MAn as a matrix and the PP as the dispersed phase, produced a fitted value of $\sigma = 1$ mN/m (Fig. 8b). This is not significantly different from the estimates derived from the unfilled blend, suggesting that the presence of clay does not affect interfacial properties.

3.2. PP rich blends

We have also studied the inverse system, in which PP forms an unfilled matrix and EPR-*g*-MAn exists as a clay-reinforced, dispersed phase. A molten 30/70 EPR-*g*-MAn/PP blend was mixed to yield a stable morphology (Fig. 9a), at which point NR_4^+-MM was charged into the system. Within 1 min of filler compounding, clay partitioned within dispersed phase droplets in the form of small tactoids and exfoliated platelets (Fig. 9b). Continued processing increased the extent of mineral exfoliation and generated particles of increasingly irregular shape (Fig. 9c–e). It should be noted that in spite of the high concentration of NR_4^+-MM in the dispersed phase, large amounts of exfoliated clay, alongside intercalated tactoids, are evident in high magnification TEM images (Fig. 9d).

The enhanced coalescence observed in the PP rich blend system is likely due to stiffening of the dispersed droplets in the presence of high amounts of exfoliated NR_4^+-MM. Inhibited particle break-up may shift the ''equilibrium'' that governs blend morphology toward increased particle coalescence rates. Hong et al. [13] attributed similar observations to the reduced deformability of the dispersed droplets, caused by their increased modulus in the presence of clay. On the contrary, enhancements in the break-up of elongated threads of the dispersed polymer have been reported in the case of the dispersed phase containing non-exfoliated clay [15]. The state of clay exfoliation in the dispersed phase therefore determines to a large extent its influence on the final blend morphology.

4. Conclusions

Filler migration in the functionalized phase takes place during the initial stages of compounding upon the addition of organically modified montmorillonite clay in an immiscible EPR-*g*-MAn/PP blend. Furthermore, the clay exfoliates to a large extent right from the onset of compounding and influences the rheological properties of the blends. In the presence of exfoliated clay in the blend matrix, substantial reductions in the size of the dispersed phase ensue; these are attributed to an enhanced droplet break-up capability, as well as a suppressed coalescence rate. On the contrary, presence of clay in the dispersed phase results in reduced capability for particle break-up and a higher tendency for coalescence, resulting in the appearance of irregular particles.

Acknowledgements

Financial support received from the Emerging Materials Knowledge (EMK) program of the Ontario Centres of Excellence (OCE)/Centre for Materials and Manufacturing, and the Natural Sciences and Engineering Research Council (NSERC) is gratefully acknowledged. Materials were kindly supplied by E.I. DuPont Canada Company and ExxonMobil. The authors would also like to thank Mr. Doug Holmyard at Mt. Sinai Hospital, Toronto, for his assistance with TEM imaging.

References

[1] Ray SS, Pouliot S, Bousmina M. Macromol Rapid Commun 2005; 26(6):450–5.
[2] Lee H, Fasulo PD, Rodgers WR, Paul DR. Polymer 2005;46(25):11673–89.
[3] Gonzalez I, Eguiazabal JI, Nazabal J. J Polym Sci Part B Polym Phys 2005;43(24):3611–20.
[4] Ray SS, Pouliot S, Bousmina M, Utracki LA. Polymer 2004;45(25): 8403–13.
[5] Khatua BB, Lee DJ, Kim HY, Kim JK. Macromolecules 2004; 37(7):2454–9.
[6] Mehta S, Mirabella FM, Rufener K, Bafna A. J Appl Polym Sci 2004;92(2):928–36.
[7] Mehrabzadeh M, Kamal MR. Polym Eng Sci 2004;44(6):1152–61.
[8] Li Y, Shimizu H. Polymer 2004;45(22):7381–8.
[9] Zhang Q, Yang H, Fu Q. Polymer 2004;45(6):1913–22.
[10] Gelfer MY, Song HH, Liu L, Hsiao BS, Chu B, Rafailovich M, et al. J Polym Sci Part B Polym Phys 2003;41(1):44–54.
[11] Wang Y, Zhang Q, Fu Q. Macromol Rapid Commun 2003;24(3):231–5.
[12] Voulgaris D, Petridis D. Polymer 2002;43(8):2213–8.
[13] Hong JS, Namkung H, Ahn KH, Lee SJ, Kim C. Polymer 2006;47(11):3967–75.
[14] Dasari A, Yu ZZ, Mai Y-W. Polymer 2005;46(16):5986–91.
[15] Dharaiya DP, Jana SC. J Polym Sci Part B Polym Phys 2005; 43(24):3638–51.
[16] Chow WS, Mohd Ishak ZA, Karger-Kocsis J, Apostolov AA, Ishiaku US. Polymer 2003;44(24):7427–40.
[17] Lipatov YS, Nesterov AE, Ignatova TD, Nesterov DA. Polymer 2002;43(3):875–80.
[18] Karim A, Liu DW, Douglas JF, Nakatani AI, Amis EJ. Polymer 2000;41(23):8455–8.
[19] Austin JR, Kontopoulou M. Polym Eng Sci 2006;46(11):1491–501.
[20] Sumita M, Sakata K, Asai S, Miyasaka K, Nakagawa H. Polym Bull 1991;25(2):265–71.
[21] Gubbels F, Jérôme R, Vanlathem E, Deltour R, Blancher S, Brouers F. Chem Mater 1998;10(5):1227–35.
[22] Everaert V, Aerts L, Groeninckx G. Polymer 1999;40(24):6627–44.
[23] Fortenly I, Zivny A. Polymer 1995;36(21):4113–8.
[24] Fortenly I, Zivny A. Polymer 1998;39(12):2669–75.
[25] Yu W, Zhou C, Inoue T. J Polym Sci Part B Polym Phys 2000; 38(18):2378–89.
[26] Yu W, Zhou C, Inoue T. J Polym Sci Part B Polym Phys 2000;38(18):2390–9.
[27] Ren J, Casanueva BF, Mitchell CA, Krishnamoorti R. Macromolecules 2003;36:4188–94.
[28] Galgali G, Ramesh C, Lele A. Macromolecules 2001;34:852–8.
[29] Aranguren MI, Mora E, DeGroot Jr JV, Macosko CW. J Rheol 1992;36(6):1165–82.
[30] Palierne JF. Rheol Acta 1990;29(3):204–14.
[31] Graebling D, Muller R, Palierne JF. Macromolecules 1993;26(2):320–9.